



Quantifying the Error Associated with the Elastic Halfspace Assumption in Site Response Analysis

Ashly Cabas, A.M.ASCE¹; Adrian Rodriguez-Marek, M.ASCE²; Russell A. Green, F.ASCE³; and Chunyang Ji, M.ASCE⁴

Abstract: One of the fundamental decisions when performing one-dimensional (1D) site response analyses (SRA) involves the selection of the depth and dynamic properties of the elastic halfspace (EHS). This boundary condition assumes linear and homogenous material underlying the soil column for an infinite depth. This assumption implies that waves refracted into the EHS are fully absorbed, and as a result, energy from waves that are potentially reflected back toward the surface from deeper impedance contrasts in the actual geologic profile are not accounted for in the SRA. If a strong soil-rock seismic impedance contrast is present at the site of interest, the EHS boundary is typically set at that depth. However, the actual geologic profile below this impedance contrast may not be in accord with the assumed properties of the EHS, which can lead to systematic errors in the SRA. An analytical expression to quantify these errors is derived in this study, verified using an idealized three-layer profile, and compared to case studies of nine real sites in Charleston, South Carolina. Our results show that the presence of a single strong impedance contrast does not suffice as the sole condition to define the EHS boundary. Frequency-dependent errors in site amplification associated with the assumptions inherent to the EHS used in the SRA can be evaluated as a function of multiple impedance contrasts present in the profile. Smaller errors are associated with strong impedance contrasts at shallower layers and/or minimal impedance contrast among layer interfaces at depth. We also find that strong impedance contrasts located at great depths within deep soil deposits introduce nonnegligible errors to site response results. DOI: 10.1061/(ASCE)GT.1943-5606.0002893. © 2022 American Society of Civil Engineers.

Introduction

The boundary condition at the base of a profile in a numerical site response analyses (SRA) is often modeled as an elastic halfspace (EHS). An EHS implies linear and homogenous material for an infinite depth below the top of the EHS, and as a result, it is assumed that waves refracted into the EHS are fully dissipated; this is also referred to as an absorbing boundary condition. The assumptions inherent to including an EHS in a numerical model are typically satisfied by the presence of hard rock (sometimes called seismic bedrock, Régnier et al. 2014) in the profile because additional impedance contrasts below the top of the hard rock are not likely (due to the high shear-wave velocity, V_s , of these materials). However, positioning and properties of the EHS used in SRA are not always consistent with actual field conditions. The main objectives of this study are to quantify the errors in SRA associated with the positioning and properties of the EHS, and to provide recommendations in this regard for defining the EHS boundary such that errors are minimized.

¹Assistant Professor, North Carolina State Univ., 915 Partners Way, Fitts-Woolard Hall, Room 3175, Raleigh, NC 27607 (corresponding author). ORCID: https://orcid.org/0000-0002-1039-4053. Email: amcabasm@ncsu.edu

Note. This manuscript was submitted on July 21, 2020; approved on May 31, 2022; published online on August 8, 2022. Discussion period open until January 8, 2023; separate discussions must be submitted for individual papers. This paper is part of the *Journal of Geotechnical and Geoenvironmental Engineering*, © ASCE, ISSN 1090-0241.

Selecting the appropriate depth and properties of the EHS for one-dimensional (1D) SRA often requires engineers to overcome hurdles related to the subsurface characterization of a site. These hurdles, which can arise from budgetary and/or technological constraints, can hinder the proper identification of the depth in the profile in which the assumptions inherent to an EHS are met. Selection of the depth and dynamic properties of the EHS can also prove challenging in profiles that have velocity reversals at depths below sharp impedance contrasts that are typically used to define the location of the EHS. Appropriate V_s site characterization is required to obtain unbiased SRA results, including the characterization of potential velocity gradients with depth and the identification of seismic impedance discontinuities capable of generating additional amplification at the site (Poggi et al. 2017), even when these occur at depths larger than those of traditional geotechnical site characterization. Furthermore, the EHS boundary condition at a site must be accompanied by the selection of input ground motions that are compatible with the assumed EHS properties (Cabas and Rodriguez-Marek 2017). However, the lack of motions recorded on hard rock (e.g., with a small-strain V_s timeaveraged over the upper 30 m, $V_{s30} > 1,500$ m/s) imposes yet

This paper examines cases in which the positioning and properties of the EHS affects the accuracy of 1D SRA. To this end, the influence of site characteristics is investigated to provide guidance regarding the use of EHS in numerical SRA. First, we introduce the challenges in the definition of reference rock conditions for SRA. Then, an analytical formulation is derived to quantify the error associated with the EHS assumption in SRA and is verified using one-dimensional SRA on idealized three-layer profiles with varying layer thickness, V_s , and damping. Errors in SRA associated with EHS assumptions are then evaluated for more complex stratigraphies using case studies of deep soil sites located in Charleston, South Carolina.

²Professor, Virginia Tech, 214 Patton Hall, Blacksburg, VA 24061. Email: adrianrm@vt.edu

³Professor, Virginia Tech, 120B Patton Hall, Blacksburg, VA 24061. Email: rugreen@vt.edu

⁴Postdoctoral Researcher, North Carolina State Univ., 915 Partners Way, Fitts-Woolard Hall, Raleigh, NC 27607. ORCID: https://orcid.org/0000-0002-9471-560X. Email: cji3@ncsu.edu

Background

Elastic Halfspace Assumption

The inclusion of an EHS in a numerical site response model implies that there is a material at depth in the geologic profile, which is sufficiently stiff such that it responds linearly to the seismic excitation, and no deeper material impedance contrasts are present (i.e., the assumption of a fully absorbent boundary is justified). Thus, the selection of a reference rock horizon as the EHS boundary in a numerical SRA implies that a portion of the elastic energy of downward propagating seismic waves will be completely absorbed by the rock mass (i.e., effectively removed from the response of the overlying soil layers). This form of radiation damping will not occur in situ if the bedrock is not homogeneous, in which case some of the energy of downward-traveling waves transmitted into the bedrock will be reflected back up from deeper impedance boundaries. Thus, modeling the inhomogeneous bedrock as an EHS means that elastic energy from these reflected waves in the actual profile does not contribute to the profile's response in the numerical SRA. In contrast, if the assumptions associated with an EHS are satisfied, the ratio of the absorbed and reflected waves becomes entirely a function of the impedance contrast between the materials on either side of the EHS boundary (e.g., Kramer 1996).

There is still no consensus on the specific properties of geologic structures that can be idealized as an EHS in the context of 1D SRA (e.g., Cadet et al. 2010; Laurendeau et al. 2013). An example of this lack of consensus is given in Table 1, which presents the characteristics of reference rock conditions found in literature and official regulations from around the world. For this reason, the characterization of a geologic profile in support of a 1D SRA should ideally include the V_s profile and attenuation characteristics of the material below the assumed position of the EHS boundary, in addition to its density (e.g., Kramer 1996).

Reference Rock and Decoupling in Site Response Analysis

The ground motions experienced at the surface of a geologic profile are a function of source, travel path, local site, and topographic effects. Seismological models treat the effects related to the wave amplification resulting from crustal velocity gradients and near-surface, distance-independent attenuation (often parameterized by the high-frequency spectral decay parameter kappa, κ) as the linear response of the upper few kilometers of the crust (Boore 2003). On the other hand, geotechnical engineers evaluate the impact of near-surface geologic deposits on ground motions, often focusing on the effects of the linear and nonlinear response of the soils overlying bedrock. Geotechnical SRA typically assume that the input motion can be applied at the bedrock underlying these deposits. This

necessarily implies a decoupling of the contributions of strata below the assumed reference depth (modeled as an EHS in the numerical SRA) from the shallower layers.

This decoupling means that the effects of wave propagation in materials below the assumed EHS boundary are not directly captured in numerical analyses of site response; therefore, these effects must be represented in the selected input motions. Toward this end, the input motions must be compatible with the profile below the assumed EHS boundary (i.e., there is reasonable agreement between the small-strain V_s profiles and attenuation characteristics of the profile at the site where the motions were recorded and those below the selected positioning of the EHS boundary: Cabas and Rodriguez-Marek 2017). Despite the proliferation of strong ground motion recordings worldwide, it can be difficult to find recordings that satisfy this agreement (e.g., Markham et al. 2016). Moreover, when the EHS boundary is placed at great depths within layers having high V_s values, the number of compatible recordings is significantly reduced [e.g., at Central-Eastern US (CEUS) sites, where the V_s of bedrock is on average 3,000 m/s: Hashash et al. 2014].

Decoupled SRA can also be performed as a two-step process, in which the response of a certain portion of the profile is first assessed up to the top of a horizon of interest, and then the rest of the profile (up to the ground surface) is analyzed. This can occur in practice when the deeper portion of the geologic profile is uniform across a region, but the shallower deposits vary significantly. In this case, it might be desirable to perform SRA of the deeper portion of the profile up to a regionally common horizon. Subsequently, SRA can be performed for the upper portion of the profile for sites of interest within the region. More commonly, the implicit assumption of a decoupled analysis is invoked when the input motions for SRA are scaled to the motions predicted by a ground motion model for the properties of the assumed EHS. In this case, the site response implicit in the ground motion model is assumed to be decoupled from the response predicted subsequently by the SRA.

While decoupled analyses are common practice, the degree to which they introduce errors in the estimation of site response has received rather limited attention to date. Likewise, the epistemic uncertainty they add to the analysis of seismic hazards is usually overlooked (e.g., Ulmer et al. 2021). Schematic representations of full and decoupled site response models (in which the SRA of a full profile model is hereafter referred to as full column analysis) are shown in Fig. 1. Knowledge of the V_s profile for the full column depicted in Fig. 1 would allow the EHS horizon to be located at the soft rock/hard rock interface (i.e., Point C). However, V_s data are often available only down to the first strong impedance contrast encountered at a site, which in this case would result in the EHS boundary being located at the interface between soil and the softer rock (i.e., Point B). The positioning of the assumed EHS boundary at either of these interfaces does not constitute a problem,

Table 1. Main properties of reference rock sites in selected building codes and publications

Reference	Definition of reference rock conditions					
Japanese regulations (Japan Road Association 1980, 1990)	$V_{s30} > 600 \text{ m/s}$					
Boore and Joyner (1997) generic rock sites	$V_{s30} > 620$ m/s and $\kappa_0 = 0.04$ s—rock sites (mostly in western North America)					
	$V_{s30} > 2,000$ m/s and $\kappa_0 < 0.01$ s—very hard rock sites (mostly in					
	eastern North America)					
National Earthquake Hazard Reduction Program (NEHRP)	$V_{s30} > 760 \text{ m/s}$ —rock sites $V_{s30} > 1,500 \text{ m/s}$ —very hard rock sites					
(Building Seismic Safety Council 2000)						
European Regulations [Eurocode 8 (CEN 2004)]	$V_{s30} > 800 \text{ m/s}$					
New Zealand Standard Structural Design Actions (SNZ 2004)	$V_{s30} > 360 \text{ m/s}$					
Cadet et al. (2010)	$750 < V_{s30} < 850$ m/s and $f_0 > 8$ Hz—standard reference rock site					
Chilean regulations (NCH 433 mod. D.S. Nº 61 MINVU 2011)	$V_{s30} > 500$ m/s—soft rock or fractured rock $V_{s30} > 900$ m/s—rock sites, cemented soils					
Hashash et al. (2014)	2,700 m/s < V_s < 3,300 m/s and κ_0 = 0.006 s (for Central and Eastern North America)					

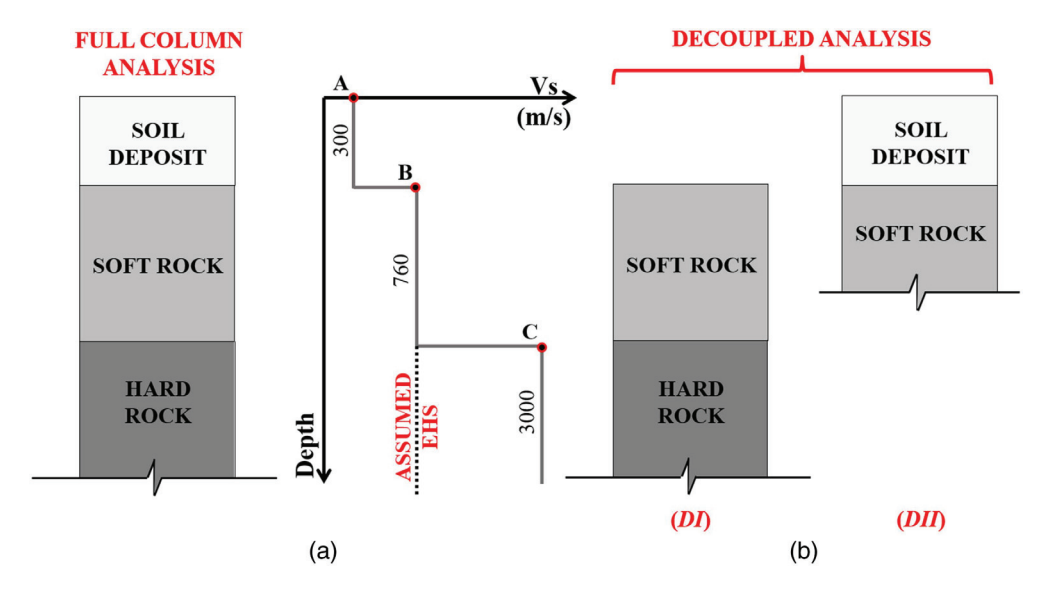


Fig. 1. (a) Full column profile with its (b) corresponding decoupled representation (*DI* and *DII* profiles). A theoretical shear wave velocity profile for the site is also shown for reference.

per se, when performing SRA, as long as the selected input motions are compatible with the assumptions inherent to the positioning of the EHS boundary in each case (i.e., recorded at a site with a similar V_s profile and attenuation characteristics as the strata below the assumed EHS boundary). In this paper, we investigate discrepancies in site response estimates as a result of different EHS assumptions. The next sections describe an analytical approach to evaluate these discrepancies and an implementation of this approach for idealized sites and real soil profiles with more complex stratigraphies.

Methodology

We compare results from full column and decoupled SRA (Fig. 1) to evaluate the effects of the geologic profile below the assumed EHS boundary. This comparison cannot be made directly because the input motions must be compatible with the assumed EHS properties in each case. Hence, we investigate the agreement between transfer functions (TFs) [defined as the ratio of Fourier amplitude spectra (FAS) between the input and the output motion in SRA] for full column and decoupled models using the classic analytical procedure for linear-elastic SRA as outlined in Kramer (1996), among others. The effects of nonlinear soil behavior are not analyzed herein but will be the focus of future investigations.

Linear-elastic SRA are performed using the analytical solution for wave propagation in a layered medium (e.g., Kramer 1996). This approach is based on the vertical propagation of horizontally polarized shear waves through horizontally layered near-surface materials. All layers are assumed to be of infinite lateral extent and both upward and downward propagating waves are considered in the estimation of the TF in the frequency domain. Commonly used software such as SHAKE (Schnabel et al. 1972; Idriss and Sun 1992), Strata (Kottke and Rathje 2008a, b), or DEEPSOIL (Hashash et al. 2015) apply this method either using 1D equivalent-linear

(EQL) (e.g., SHAKE, Strata, and DEEPSOIL) or nonlinear (NL) approaches in the time domain (e.g., DEEPSOIL) to model the shear stress-shear strain behavior of soil under cyclic loading.

The three-layer profile shown in Fig. 1 is used to introduce the mathematical formulation of the TF for the full column and decoupled models. The TF for the *full column* is defined as the ratio of the acceleration FAS of the motions at the surface and soft rockhard rock interface

$$(TF)_{FULL} = \frac{FAS_{Surface}}{FAS_{HardRock}}$$
 (1)

where FAS refers to the acceleration Fourier amplitude spectrum of outcrop ground motions at the top of the layer indicated by the subscript. Meanwhile, the TF for the *decoupled model*, $(TF)_{DEC}$, is defined by the product of the corresponding amplifications for each decoupled profile, DI and DII, as presented in Fig. 1(b)

$$(TF)_{DEC} = \frac{FAS_{SoftRock}}{FAS_{HardRock}} \cdot \frac{FAS_{Surface}}{FAS_{SoftRock}}$$
(2)

To solve for $(TF)_{FULL}$ and $(TF)_{DEC}$, the solution to the wave equation (e.g., Kramer 1996) is used, which considers upward and downward propagating waves in a layered medium to estimate displacements (u) at a depth z and time t

$$u_j(z,t) = A_j e^{i(\omega t + k_j h_j)} + B_j e^{-i(\omega t + k_j h_j)}$$
(3)

where A_j and B_j = amplitudes of upgoing and downgoing waves, respectively, in the jth layer having an angular frequency ω ; k_j = wave number of the jth layer and can be expressed as $\omega/V_{s,j}$; and h_j = thickness of the jth layer. Note that TFs for accelerations, velocities, and displacements are identical (e.g., Kramer 1996). Analytical expressions for the wave amplitudes within the idealized three-layer full column model in matrix form are

$$\begin{bmatrix} A_{HR} \\ B_{HR} \end{bmatrix} = \begin{bmatrix} \frac{1}{2} (1 + \alpha_{SR}) e^{ik_{SR}h_{SR}} & \frac{1}{2} (1 - \alpha_{SR}) e^{-ik_{SR}h_{SR}} \\ \frac{1}{2} (1 - \alpha_{SR}) e^{ik_{SR}h_{SR}} & \frac{1}{2} (1 + \alpha_{SR}) e^{-ik_{SR}h_{SR}} \end{bmatrix} \begin{bmatrix} \frac{1}{2} (1 + \alpha_{S}) e^{ik_{S}h_{S}} & \frac{1}{2} (1 - \alpha_{S}) e^{-ik_{S}h_{S}} \\ \frac{1}{2} (1 - \alpha_{S}) e^{ik_{S}h_{S}} & \frac{1}{2} (1 + \alpha_{S}) e^{-ik_{S}h_{S}} \end{bmatrix} \begin{bmatrix} 1 \\ 1 \end{bmatrix} A_{S}$$

$$(4)$$

where the subscripts HR, SR, and S = hard rock, soft rock, and soil layers, respectively, shown in Fig. 1 for the three-layer idealized full column model. The α terms correspond to seismic impedance contrasts at each layer boundary and are computed as (e.g., Kramer 1996)

$$\alpha_{\frac{layer1}{layer2}} = \frac{(\rho V_s)_{layer1}}{(\rho V_s)_{layer2}} \tag{5}$$

where layer 1 overlies layer 2; ρ = mass density; and V_s = shear-wave velocity. The terms α_{SR} and α_S in Eq. (4) correspond to the impedance contrasts between the soft and hard rock (i.e., α_{SR}), and

between the soil layer and the soft rock (i.e., α_S). Solving Eq. (4) requires estimating the coefficients A and B that satisfy the boundary conditions of the problem

$$(TF)_{FULL} = \frac{(A_S + B_s)}{(A_{HR} + B_{HR})}$$
 (6)

where $A_S = B_S$ due to the stress-free boundary condition at the ground surface.

Outcropping conditions (i.e., stress-free boundary condition) are also assumed at the top of the hard rock layer. Hence, the denominator in Eq. (6) becomes $2A_{HR}$. Substituting Eq. (4) into Eq. (6) and simplifying the results

$$(TF)_{FULL} = \frac{1}{\cos(\frac{\omega h_{SR}}{V_{SR}})\cos(\frac{\omega h_S}{V_S}) - \alpha_S\sin(\frac{\omega h_{SR}}{V_{SR}})\sin(\frac{\omega h_S}{V_S}) + i\alpha_{SR}\sin(\frac{\omega h_{SR}}{V_{SR}})\cos(\frac{\omega h_S}{V_S}) + i\alpha_{SR}\alpha_S\sin(\frac{\omega h_S}{V_S})\cos(\frac{\omega h_{SR}}{V_S})}$$
(7)

where the subscripts HR, SR, and S = hard rock, soft rock, and soil layers, respectively; and V = shear-wave velocity for the corresponding layer (i.e., HR, SR, or S). Similarly, solving for $(TF)_{DEC}$ using the same expressions (and boundary conditions) for upgoing and downgoing propagating waves in a layered medium

$$(\text{TF})_{DI}(\omega) = \frac{1}{\cos(\frac{\omega h_{SR}}{V_{CR}}) + i\alpha_{SR}\sin(\frac{\omega h_{SR}}{V_{CR}})}$$
(8)

$$(TF)_{DII}(\omega) = \frac{1}{\cos(\frac{\omega h_S}{V_a}) + i\alpha_S \sin(\frac{\omega h_S}{V_a})}$$
(9)

$$(\text{TF})_{\text{DEC}} = \frac{1}{\left[\cos\left(\frac{\omega h_{SR}}{V_{SR}}\right) + i\alpha_{SR}\sin\left(\frac{\omega h_{SR}}{V_{SR}}\right)\right]} \cdot \frac{1}{\left[\cos\left(\frac{\omega h_{S}}{V_{S}}\right) + i\alpha_{S}\sin\left(\frac{\omega h_{S}}{V_{S}}\right)\right]}$$
(10)

We define the transfer function ratio (TFR) as the ratio of the TF for the full column and decoupled models. This parameter quantifies the differences in 1D SRA as a function of the EHS assumption

$$TFR = \frac{(TF)_{FULL}}{(TF)_{DEC}} \tag{11}$$

The numerator and denomintor in Eq. (11) result from Eqs. (7) and (10), respectively. A TFR of unity implies that the shallow impedance contrast can be safely assumed to be the location of the EHS boundary condition. Substituting Eqs. (7) and (10) into Eq. (11), and substituting $\theta_S = \omega h_S/V_S$ and $\theta_{SR} = \omega h_{SR}/V_{SR}$, an analytical expression for TFR can be derived

$$TFR = \frac{\cos(\theta_S)\cos(\theta_{SR}) - \alpha_{SR}\alpha_S\sin(\theta_S)\sin(\theta_{SR}) + i\alpha_{SR}\cos(\theta_S)\sin(\theta_{SR}) + i\alpha_S\sin(\theta_S)\cos(\theta_{SR})}{\cos(\theta_S)\cos(\theta_{SR}) - \alpha_S\sin(\theta_S)\sin(\theta_{SR}) + i\alpha_{SR}\cos(\theta_S)\sin(\theta_{SR}) + i\alpha_{SR}\alpha_S\sin(\theta_S)\cos(\theta_{SR})}$$
(12)

Adding the terms $\pm \alpha_S \sin(\theta_S) \sin(\theta_{SR})$ and $\pm i\alpha_{SR}\alpha_S \sin(\theta_S) \cos(\theta_{SR})$ to the numerator of Eq. (12) leaves it unchanged, but it can be rewritten as

$$TFR = \frac{[(TF)_{FULL}]^{-1} + [\alpha_S(1 - \alpha_{SR})\sin(\theta_S)\sin(\theta_{SR})] + i[\alpha_S(1 - \alpha_{SR})\sin(\theta_S)\cos(\theta_{SR})}{[(TF)_{FULL}]^{-1}}$$
(13)

Further rearrangement of terms including the use of Euler's law and taking the absolute value of the complex number results in

$$|TFR - 1| = |(TF)_{FULL}|\alpha_S(1 - \alpha_{SR})\sin(\theta_S)$$
 (14)

Eq. (14) is a measure of the TFR's departure from unity and demonstrates analytically that the error in site response associated with the truncation of the soil profile is a function of the impedance contrast at shallow and deeper layers (i.e., between the soil and soft rock layer, α_S , as well as between the soft and hard rock layers, α_{SR} , in this case), the thickness and V_S of the materials, and wavelengths

considered. For example, the outcome of Eq. (14) will be small (i.e., TFR \approx 1) if:

- 1. $|(TF)_{FULL}| \ll 1$, which happens for very high frequencies.
- 2. $\alpha_S \ll 1$, which results from the soft rock layer being much stiffer than the overlying soil layer.
- 3. $\alpha_{SR} \approx 1$, which means that there is barely a contrast between the soft and hard rock layers.
- 4. $\sin(\theta_S) \approx 0$, which leads to $\theta_S \approx m\pi$ for $m = 0, 1, 2 \dots$ where $\theta_S = \omega h_S/V_S$
 - a. m = 0 corresponds to the case of very low frequencies (i.e., long wavelengths propagating through the soil stratum).

© ASCE 04022081-4 J. Geotech. Geoenviron. Eng.

b. m > 0 corresponds to wavelengths in the soil stratum equal to $2h_S, h_S, h_S/2, \ldots$, (as θ_S can be written as a function of wavelength and layer thickness, $\theta_S = 2\pi h_S/\lambda_S$), which represent cases in which the free-surface and the interface move the same way. This factor accounts for scenarios in which the propagating wave makes the deformation of the soil layer appear as a rigid body motion, since its extremes move in the same fashion.

For scenarios in which none of the aforementioned conditions (i.e., Items 1–4) are met, the $(TF)_{DEC}$ will incur significant errors (i.e., $TFR\gg1$). These inferences are further verified with a parametric study described in the next section. The results of the parametric study are then compared to the results of a case study corresponding to real sites in Charleston, South Carolina.

Analysis of an Idealized Three-Layer Model

Based on Eq. (14), the errors associated with the assumed characteristics and positioning of the EHS can be evaluated as a function of the impedance contrast at shallow (α_S) and deeper layers (α_{SR}), the thicknesses (h_S and h_{SR}), and shear-wave velocities (V_S and V_{SR}) of the materials. These factors can control the amplitude and time of arrival of potential reflected waves coming from deeper layer boundaries within the profile being analyzed.

The analyses presented herein are designed as a verification exercise using the three-layer model depicted in Fig. 1, consisting of a soil layer and a soft rock layer overlying hard bedrock. Variations in the V_s and minimum shear strain damping ratio (ξ_{\min}) of all three layers, as well as variations in the thicknesses of the soil and soft rock layers, are used to further investigate discrepancies between the TFs of full column and decoupled models. The range of values considered is listed in Table 2. Only one layer property in the site profile is changed at a time. Also, only profiles with increasing V_s with depth are investigated (i.e., no velocity reversals are considered). A subset of computed TFR values is depicted in Fig. 2 (using linear-elastic site amplifications) for variations in the V_s of the soil layer [Fig. 2(a)], V_s of the soft rock layer [Fig. 2(b)], V_s of the hard rock layer [Fig. 2(c)], and thickness of the soft rock layer, h_{SR} [Fig. 2(d)]. The baseline case used in Fig. 2 comprises a 50-m-thick uniform soil layer with V_s of 300 m/s, a 50-m-thick uniform soft rock layer with a V_s of 760 m/s, and a hard rock stratum with V_s of 3,000 m/s.

First, it is observed that TFR values are equal to 1 for very low frequencies and approach unity again for high frequencies in all cases shown in Fig. 2. These results are consistent with inferences made from Eq. (14) [i.e., Items 1 and 4 in the discussion following Eq. (14)]. For the baseline case shown in Fig. 2(a), the impedance ratio for the soft and hard rock strata, α_{SR} , is 0.25. As the impedance ratio between the soil and the underlying soft rock, α_{S} , decreases [i.e., as the soil layer becomes significantly softer; depicted by darker curves in Fig. 2(a)], decoupled and full column analyses render more similar first mode site responses. This is consistent with

Table 2. Range of values considered in the parametric study performed on a three-layer soil profile comprised of a soil deposit overlying soft rock and hard rock layers

Site property	Soil	Soft rock	Hard rock
Unit weight (kN/m ³)	20	27.5	27.5
Vs (m/s)	100-760	760-3,000	760-3,000
Thickness (m)	50, 100, 250	50, 100, 250	_
Minimum shear strain damping (%)	2.0–10.0	1.0-5.0	0.5–3.0

Eq. (14), in which scenarios with $\alpha_S < 1$ render TFR closer to unity. However, full column analyses result in first mode amplifications that are at least 50% larger than the decoupled analysis even for the softest soil conditions analyzed. This observation can also be explained by Eq. (14) because the error associated with the EHS assumption is not only a function of α_S , but other parameters as well

As the V_s of the soft rock increases [i.e., α_{SR} increases from 0.25 to 1, which corresponds to the progressively lighter curves in Fig. 2(b)], approaching the V_s of the underlying hard rock, TFR values decrease. When the V_s of the soft and hard rock layers are equal, TFR is equal to one across all frequencies, which is expected because the EHS assumptions of homogeneity and elasticity are fulfilled in this case. These observations align well with Item 3 in the discussion following Eq. (14), which describes scenarios in which there is barely a contrast between the soft and hard rock layers ($\alpha_{SR} \approx 1$). Lower values of V_s in the soft rock layer lead to stronger impedance contrasts at the interface with the hard rock layer (i.e., smaller values of α_{SR} that further deviate from 1). Such condition generates increasingly significant differences between the full column and the decoupled models [e.g., darker curves in Fig. 2(b)]. Analogously, increasing the V_s of the hard rock layer [i.e., α_{SR} decreases from 1 to 0.25, which corresponds to the progressively lighter curves in Fig. 2(c)] results in larger amplifications for the full column analysis (i.e., larger TFR values). In this case, amplifications for the full column analysis are more than twice as high as the amplifications obtained for the first mode in the decoupled analysis. However, in this case, varying the V_s of the hard rock layer does not result in a frequency shift of the loci of the maximum TFR values.

We also investigate the influence of the depth of the boundary between the soft and hard rock by increasing the thickness of the soft rock layer, h_{SR} , because it affects the value of $(TF)_{FULL}$ at low frequencies. The resulting shift in resonant frequency of the full column profile as compared to its decoupled counterpart can introduce errors in estimated TFs. Fig. 2(d) depicts the differences between TFs from full column and decoupled models, when varying h_{SR} , from 50 to 250 m. Larger values of h_{SR} imply that the strong impedance contrast between the soft and hard rock layers is located deeper within the profile (note: $\alpha_{SR} = 0.25$ for all values of h_{SR} considered). Two key observations result from Fig. 2(d). First, the TFR value for the first resonant mode [i.e., the first peak in the TFR curve in Fig. 2(d)] decreases as the depth of the impedance boundary between the soft and hard rock increases within the profile. Second, a unique first mode peak obtained for the shallow impedance contrast case evolves into two distinct peaks for the same impedance contrast located at greater depths (within a similar frequency band). This observation can be explained by a shift in resonance.

Variations in $\xi_{\rm min}$ values were also explored as part of this parametric study, but the corresponding figures are not shown because assumptions of $\xi_{\rm min}$ values were found not to contribute to the errors related to the compliance with the EHS assumptions. This is also evidenced in Eq. (14) because values of $\xi_{\rm min}$ are only implicitly accounted for within the $({\rm TF})_{FULL}$ term.

Compliance with the EHS Assumptions as Evidenced in Case Studies

Previous studies have provided evidence of the influence of V_s variation at large depths on the site response of deep sedimentary profiles (e.g., Frankel et al. 2002; Park and Hashash 2004). In this study, we investigate the presence of a strong impedance contrast at large depths for nine sites located in Charleston, South Carolina.

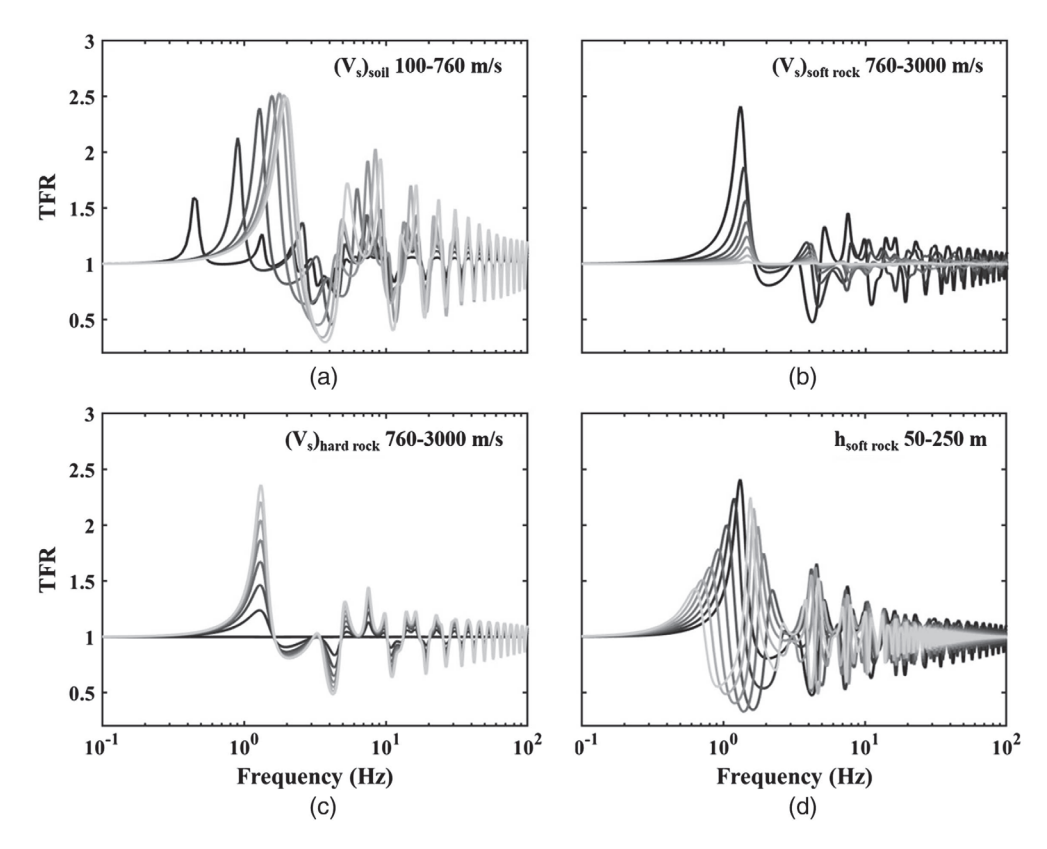


Fig. 2. A subset of selected TFR results from the parametric study performed using a three-layer model with the following varying properties: (a) V_s of the soil layer (with increments of 100 m/s); (b) V_s of the soft rock layer (with increments of 300 m/s); (c) V_s of the hard rock layer (with increments of 300 m/s); and (d) thickness of the soft rock layer (with increments of 30 m). The baseline case model consists of a 50 m-thick soil layer with a V_s of 300 m/s overlying a 50 m-thick soft rock layer with a V_s of 760 m/s, and a hard rock stratum with V_s of 3,000 m/s. Progressively lighter curves indicate increasingly stiffer materials in (a–c), while they indicate a thicker soft rock layer in (d).

These strong seismic impedance contrasts result from hard bedrock conditions (typically found in CEUS with mean V_s values of 3,000 m/s: Hashash et al. 2014) underlying deep sedimentary deposits found near the coast. An idealized depiction of this type of site profile is shown in Fig. 3(a). The strongest impedance contrast is located at a depth greater than 800 m [Fig. 3(b)], which is ignored in typical geotechnical SRA because they often only include the upper portion of the profile [e.g., top 72 m of soil deposit, represented by the idealized DII profile in Fig. 3(c)].

The study sites are close to the coast in the southeast region of South Carolina, as shown in Fig. 4 (geographic coordinates provided in Table 3). Seismic cone penetration test data are available at these sites and reveal the varying thicknesses of soil deposits and marl overlying a common sedimentary formation. In general, the soil composition is similar across sites, comprising mainly of sands and clays, but the V_s profiles slightly differ, especially in the upper 30 m.

Linear SRA are performed using Strata version 0.8.1 (Kottke and Rathje 2008a, b) on full column and decoupled models [Figs. 3(a and c)] of each study site to estimate the corresponding TFR values. A decoupling (or truncation) depth equal to 72 m is selected for most sites because of the presence of a strong impedance contrast at that depth between the soil deposits and the sedimentary rock formations (see Table 3 for specific truncation depths for each case, as indicated by the thicknesses of the soil layer or DII profile). A rather uniform V_s profile is found below 72 m for most study sites. To perform 1D linear-elastic SRA using Strata, 20 sets of ground motion records (i.e., 40 recorded horizontal orthogonal components) are selected from the Next Generation Attenuation

(NGA)-West 2 database (NGA-West 2 2013). These input motions correspond to shallow crustal earthquakes with moment magnitudes between 5 and 9, and epicentral distances ranging from 2 to 103 km (following seismic hazard deaggregation results in Charleston, South Carolina). Ground motion records from stable, continental regions would be preferred in this case, given the location of the study sites; however, design level ground motion records from the NGA-East database (Goulet et al. 2021) were not available at the time of completion of this study. Moreover, only ground motions recorded at sites with $V_{s30} > 760$ m/s were considered, but none of the selected ground motions was recorded at hard rock conditions (i.e., $V_{s30} > 1,500$ m/s).

Maximum TFR values for each site are presented in Table 3. The maximum TFR values for the first mode range from 1.32 to 1.52 (Table 3). The overall maximum TFR values are approximately 5 for all sites, with this value corresponding to a frequency of 1.46 Hz (i.e., a period of ~ 0.7 s, which is similar to T_{0_DII} , the fundamental period of the decoupled profiles presented in Table 3 ranging between 0.7 and 0.9 s, except for site CH-8). We compare the TFR values in Table 3 with those estimated for simplified profiles using Fig. 3. The actual stratigraphy in situ is used to define the three main idealized layers (i.e., soil, soft rock, and hard rock) for each study site, and the corresponding average values of V_s for each layer are reported in Table 3. It must be noted that the use of a time-averaged V_s value across a stratified profile to capture the fundamental mode behavior of the soil column of interest is not appropriate (e.g., Zhao 1997). However, in this case, the time-averaged V_s values are only used to make comparisons to the idealized threelayer profile investigated as part of our verification exercise of the

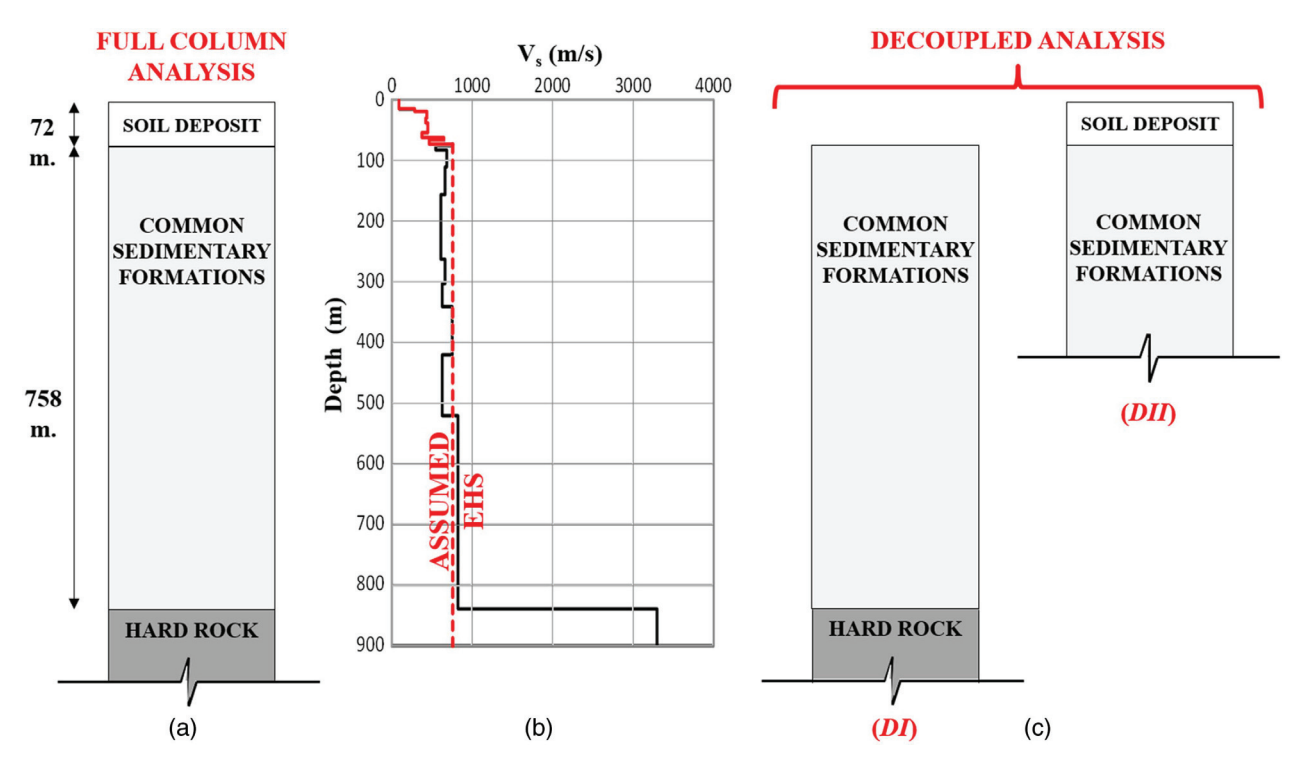


Fig. 3. (a) Full column profile corresponding to an idealized representation of the sites located in Charleston, South Carolina, with (b) a typical V_s profile of sites in the area; and (c) typical assumption for the location of the EHS (in absence of sufficient V_s data at greater depths). DI and DII refer to the corresponding decoupled profiles.

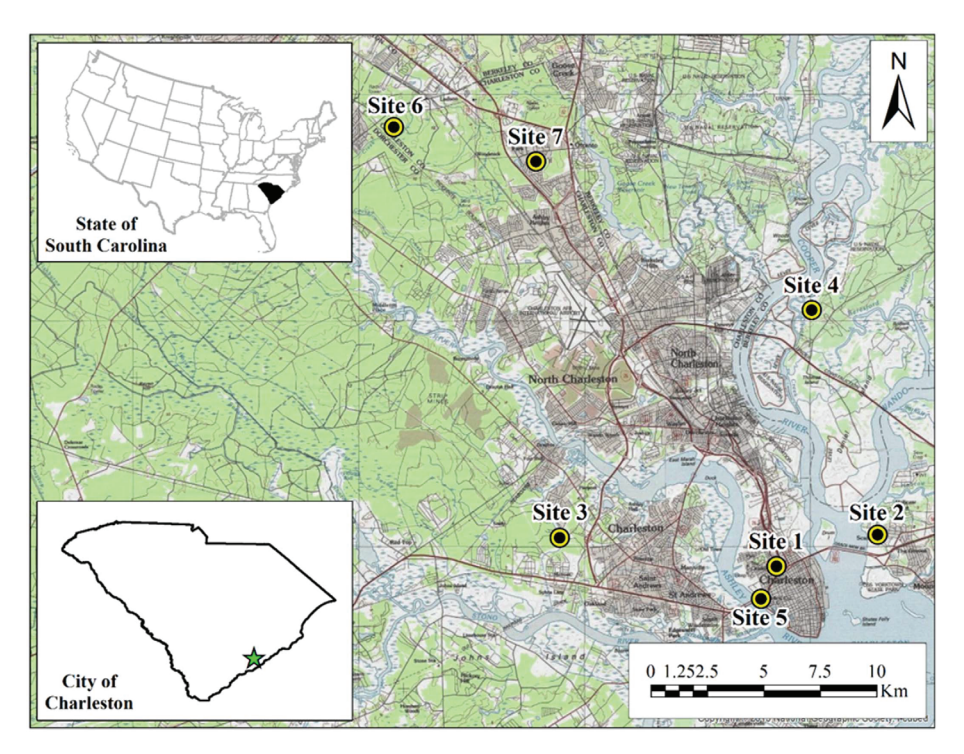


Fig. 4. Plan view of the study area. The locations of seven of the nine sites used in this study is shown. The coordinates for Sites 8 and 9 were not available at the time of completion of this study. (Reprinted from USGS Topographic Maps 2022.)

analytical expression derived for TFR [i.e., Eq. (14)]. Table 3 also presents the corresponding seismic impedance contrasts between idealized soil, soft rock, and hard rock layers, estimated fundamental periods (using the $4 \text{ H}/V_{s_avg}$ approximation), and maximum values of TFR. On average (i.e., across all study sites), α_S is 0.4,

while α_{SR} is 0.22. This means that the impedance contrast at depth is stronger than the one corresponding to shallower depth at the interface between sedimentary deposits and soft rock [i.e., smaller values of α correspond to larger density and velocity products in the denominator of Eq. (5)]. Moreover, according to Eq. (14), small errors

Table 3. Characteristics of study sites in Charleston, South Carolina, including average shear-wave velocity, seismic impedance contrast, fundamental periods, and thickness corresponding to equivalent soil, soft rock, and hard rock layers. Maximum errors calculated in terms of TFR are also provided

				$V_{s,avg}$ (m/	's)	α		T_0 (s)		Thickness (m)			TFR		
Site #	Latitude	Longitude	Soil	Soft rock	Hard rock	α_S	α_{SR}	T_{0_full}	T_{0_DII}	hs	h_{SR}	h_{full}	TFR ^a	TFR ^b	SRRc
CH-1	32.798	-79.948	322	713.6	3,300	0.33	0.22	5.1	0.9	72	758	830	1.5	5.3	1.1
CH-2	32.810	-79.900	352.5	713.6	3,300	0.36	0.22	5.1	0.8	72	758	830	1.5	5.4	1.1
CH-3	32.810	-80.050	421.9	713.6	3,300	0.43	0.22	4.9	0.7	72	758	830	1.5	5.3	1.1
CH-4	32.900	-79.930	357.6	713.6	3,300	0.36	0.22	5.2	0.9	81	758	839	1.5	5.1	1.2
CH-5	32.785	-79.955	358.8	713.6	3,300	0.37	0.22	5.1	0.8	72	758	830	1.5	5.1	1.2
CH-6	32.974	-80.127	358.6	713.6	3,300	0.37	0.22	5.1	0.9	78	758	836	1.5	5.2	1.2
CH-7	32.960	-80.060	374.6	713.6	3,300	0.38	0.22	5.0	0.8	72	758	830	1.5	5.4	1.1
CH-8	_	_	463.6	713.6	3,300	0.47	0.22	4.7	0.4	52	758	810	1.3	4.6	1.1
CH-9	_	_	379.8	713.6	3,300	0.39	0.22	5.0	0.8	72	758	830	1.5	5.4	1.2
Average	_	_	376.6	713.6	3,300	0.4	0.2	5.0	0.8	71.4	758.0	829.4	1.5	5.2	1.2

 $^{^{}a}$ Maximum TFR value corresponding to the first mode of vibration, at approximately T_{0_full} .

^cSpectral ratios ratio.

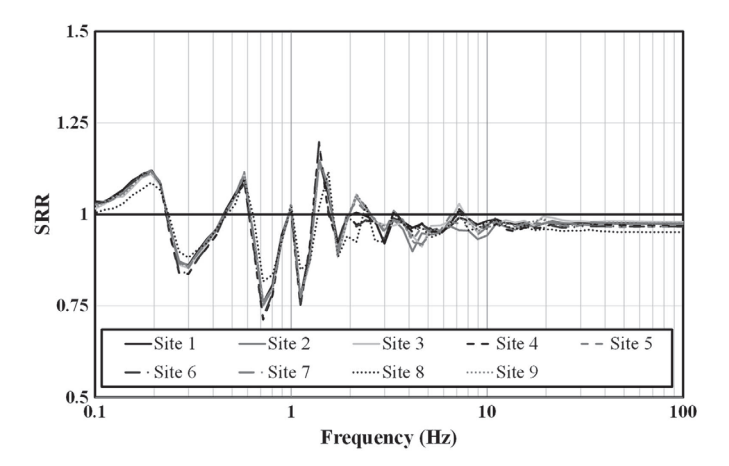


Fig. 5. Values of mean spectral ratios ratio (SRR) corresponding to all study sites in Charleston, South Carolina.

or TFR values are associated with either small $\alpha_{\rm S}$ (representing a strong impedance contrast at the interface between soils and soft rock) or with $\alpha_{\rm SR}$ closer to unity (which reflects barely any impedance contrast between the soft rock and hard rock layers). None of these conditions is satisfied for the study sites.

Errors associated with the truncation of the profile in terms of mean spectral ratios are presented in Fig. 5. Because spectral ratios are dependent on the selected input motions, the estimated errors in Fig. 5 [hereafter referred to as spectral ratios ratio (SRR)] can only serve as a reference to evaluate patterns in the data, rather than definitive measures of the error when performing decoupled SRA at the sites of interest. Spectral ratios are computed by dividing 5%-damped pseudospectral accelerations estimated at the surface by their outcrop counterparts at the assumed EHS boundary for each case. The spectral ratio corresponding to the decoupled model is defined as the product of the spectral ratios for each decoupled profile (i.e., DI and DII), analogous to Eq. (2). Values of SRR are then computed similarly to Eq. (11) by using spectral ratios instead of transfer functions. Using spectral accelerations to obtain values of SRR for all selected sites results in a smoothing effect, as illustrated in Fig. 5. All study sites provide fairly similar results in terms of SRR, and the values imply errors always less than 30%.

Conclusions

Numerical seismic site response analyses commonly involve decoupling the effects of deeper strata from the response of shallower layers. This study examined systematic errors introduced in amplification factors when the reference depth selected for numerical analysis at the site of interest does not comply with the assumptions inherent to an elastic halfspace. These assumptions imply that all the energy of downgoing propagating seismic waves, which are transmitted into the halfspace, is radiated away from the surface layers. The appropriate choices of the positioning and properties of the EHS in site response models are relevant because they also imply that the input motions applied to such boundary should be recorded at a site with an equivalent site response to that below the assumed EHS.

The linear-elastic response of an entire profile, as well as that of its decoupled representation, are used to estimate errors in site response analysis when the elastic halfspace boundary is assumed at a depth that is not geologically justified. Theoretical formulations for wave propagation in layered media were used to derive an analytical expression that quantifies the error associated with the EHS assumption in SRA [i.e., Eq. (14)]. This expression was verified by computing the corresponding 1D site amplifications for full column and decoupled models of idealized three-layer profiles. Our findings indicate that errors associated with the decoupled models are a function of the impedance contrast at shallow and deeper layers (e.g., between the soil and soft rock layer, as well as between the soft and hard rock layers, for the three-layer profiles analyzed herein), the thickness and V_s of the materials, and wavelengths considered. These factors influence the amplitude, frequency, and time of arrival of potential reflected waves coming from deeper layer boundaries within the profile under study.

Eq. (14) is proposed to help guide the otherwise subjective decision of where to locate the EHS boundary in SRA. We find that larger differences between the product of V_s and density of the soft rock materials and the overlying sedimentary deposits result in smaller errors [i.e., stronger, shallow impedance ratio leads to smaller TFR values based on Eq. (14)]. In addition, barely no impedance contrast between rock materials at depth (i.e., fairly uniform density and V_s values within the rock mass) also lead to smaller errors associated with the EHS assumption.

Case studies of deep sedimentary columns in Charleston, South Carolina, were presented to evaluate real sites and compare estimated errors associated with the truncation of the models with

^bAbsolute maximum.

findings using idealized cases. We found that the error associated with the decoupled profile is not negligible for sites with deep soil columns overlying very strong seismic impedance contrasts at depth; these conclusions are consistent with the insights gained from the derivation of TFR as a function of impedance contrasts in Eq. (14) and with the 1D SRA conducted using idealized three-layer profiles. Deep soil columns represent a significant departure from the hypotheses behind the assumptions inherent to using an EHS; ignoring the influence of the deeper portion of the profile on the overall site response can lead to nontrivial errors in the estimation of the seismic response of the site. Our findings highlight the importance of the characterization of deep V_s profiles for cases in which deep impedance contrasts are expected based on the geology and depositional environment at the site of interest. Eq. (14) can be used to evaluate cases in which additional analyses to identify the impact of profile decoupling might be needed.

Data Availability Statement

Some or all data, models, or code that support the findings of this study are available from the corresponding author upon reasonable request.

Acknowledgments

This research was partially funded by National Science Foundation (NSF) Grants CMMI-1825189 and CMMI-1937984. This support is gratefully acknowledged. Additionally, this study significantly benefited from the comments of two anonymous reviewers. However, any opinions, findings, and conclusions or recommendations expressed in this material are those of the authors and do not necessarily reflect the views of the NSF or those that provided review comments.

References

- Boore, D. 2003. "Simulation of ground motion using the stochastic method." Pure Appl. Geophys. 160 (3–4): 635–676. https://doi.org/10.1007
- Boore, D. M., and W. B. Joyner. 1997. "Site amplifications for generic rock sites." Bull. Seismol. Soc. Am. 87 (2): 327–341.
- Building Seismic Safety Council. 2000. The 2000 NEHRP recommended provisions for new buildings and other structures: Part I (Provisions) and Part II (Commentary). Technical Rep. No. FEMA 368/369. Washington, DC: Federal Emergency Management Agency.
- Cabas, A., and A. Rodriguez-Marek. 2017. "VS-κ0 correction factors for input ground motions used in seismic site response analyses." *Earth-quake Spectra* 33 (3): 917–941. https://doi.org/10.1193/22315eqs188m.
- Cadet, H., P.-Y. Bard, and A. Rodriguez-Marek. 2010. "Defining a standard rock site: Propositions based on the KiK-net database." *Bull. Seismol. Soc. Am.* 100 (1): 172–195. https://doi.org/10.1785/0120090078.
- CEN (European Committee for Standardization). 2004. Eurocode 8: Design of structures for earthquake resistance, part 1: General rules, seismic actions and rules for buildings. EN 1998-1. Brussels, Belgium: CEN.
- Frankel, A. D., D. L. Carver, and R. A. Williams. 2002. "Nonlinear and linear site response and basin effects in Seattle for the M 6.8 Nisqually, Washington, earthquake." *Bull. Seismol. Soc. Am.* 92 (6): 2090–2109. https://doi.org/10.1785/0120010254.
- Goulet, C. A., et al. 2021. "PEER NGA-east database." Supplement, *Earth-quake Spectra* 37 (S1): 1331–1353. https://doi.org/10.1177/875529302 11015695.

- Hashash, Y. M. A., A. R. Kottke, J. P. Stewart, K. W. Campbell, B. Kim, C. Moss, S. Nikolaou, E. M. Rathje, and W. J. Silva. 2014. "Reference rock site condition for Central and Eastern North America." *Bull. Seis*mol. Soc. Am. 104 (2): 684–701. https://doi.org/10.1785/0120130132.
- Hashash, Y. M. A., M. I. Musgrove, J. A. Harmon, D. R. Groholski, C. A. Phillips, and D. Park. 2015. DEEPSOIL 6.0, user manual. Urbana, IL: Univ. of Illinois at Urbana-Champaign.
- Idriss, I. M., and J. I. Sun. 1992. User's manual for SHAKE91: A computer program for conducting equivalent linear seismic response analyses of horizontally layered soil deposits. Davis, CA: Center for Geotechnical Modeling, Dept. of Civil and Environmental Engineering, Univ. of California at Davis.
- Japan Road Association. 1980. Specifications for highway bridges, Part V, Seismic Design. Tokyo: Maruzen Co., Ltd.
- Japan Road Association. 1990. Specifications for highway bridges, Part V, Seismic Design. Tokyo: Maruzen Co., Ltd.
- Kottke, A. R., and E. M. Rathje. 2008a. Strata, Version alpha, Revision 381. Austin, TX: Univ. of Texas at Austin.
- Kottke, A. R., and E. M. Rathje. 2008b. *Technical manual for strata*. Rep. No. 2008/10. Berkeley, CA: Pacific Earthquake Engineering Research Center, Univ. of California at Berkeley.
- Kramer, S. 1996. Geotechnical earthquake engineering. Upper Saddle River, NJ: Prentice Hall.
- Laurendeau, A., F. Cotton, O.-J. Ktenidou, L.-F. Bonilla, and F. Hollender. 2013. "Rock and stiff soil site amplification: Dependency on VS30 and kappa (κ0)." *Bull. Seismol. Soc. Am.* 103 (6): 3131–3148. https://doi.org /10.1785/0120130020.
- Markham, C., J. Bray, M. Riemer, and M. Cubrinovski. 2016. "Characterization of shallow soils in the central business district of Christchurch, New Zealand." *Geotech. Test. J.* 39 (6): 20150244. https://doi.org/10.1520/GTJ20150244.
- NCH 433 mod. D.S. Nº 61 MINVU. 2011. Reglamento que fja el diseño sísmico de edificios y deroga. [In Spanish.] Decreto Nº 117, de 2010. Santiago, Chile: Ministerio de Vivienda y Urbanismo.
- NGA-West 2. 2013. Next generation attenuation—West 2 database. Berkeley, CA: Pacific Earthquake Engineering Research Center.
- Park, D., and Y. M. Hashash. 2004. "Probabilistic seismic hazard analysis with nonlinear site effects in the Mississippi embayment." In *Proc.*, 13th World Conf. on Earthquake Engineering. Vancouver, BC, Canada: Canadian Association for Earthquake Engineering.
- Poggi, V., J. Burjanek, C. Michel, and D. Fah. 2017. "Seismic site-response characterization of high-velocity sites using advanced geophysical techniques: Application to the NAGRA-Net." *Geophys. J. Int.* 210 (2): 645–659. https://doi.org/10.1093/gji/ggx192.
- Régnier, J., L. F. Bonilla, E. Bertrand, and J.-F. Semblat. 2014. "Influence of the V_S profiles beyond 30 m depth on linear site effects: Assessment from the KiK-net data." *Bull. Seismol. Soc. Am.* 104 (5): 2337–2348. https://doi.org/10.1785/0120140018.
- Schnabel, P. B., J. Lysmer, and H. B. Seed. 1972. SHAKE: A computer program for earthquake response analysis of horizontally-layered sites. Rep. No. EERC-72/12. Berkeley, CA: Earthquake Engineering Research Center, Univ. of California at Berkeley.
- SNZ (Standards New Zealand). 2004. Structural design actions: Part 5 earthquake actions: New Zealand. New Zealand Standard NZS 1170.5:2004. Wellington, NZ: SNZ.
- Ulmer, K. J., A. Rodriguez-Marek, and R. A. Green. 2021. "Accounting for epistemic uncertainty in site effects in probabilistic seismic hazard analysis." *Bull. Seismol. Soc. Am.* 111 (4): 2005–2020. https://doi.org /10.1785/0120200343.
- USGS Topographic Maps. 2022. "US topo: Maps for America." Accessed July 5, 2022. https://www.usgs.gov/programs/national-geospatial-program/us-topo-maps-america.
- Zhao, J. X. 1997. "Modal analysis of soft-soil sites including radiation damping." *Earthquake Eng. Struct. Dyn.* 26 (1): 93–113. https://doi.org/10.1002/(SICI)1096-9845(199701)26:1<93::AID-EQE625>3.0.CO;2-A.